A rational catalyst design of CO oxidation usingthe bonding contribution equation

A Rational Catalyst Design of CO oxidation Using the Bonding Contribution Equation

Ziyun Wang[a] and P. Hu[a]

Rational design of heterogeneous catalysts is an important yet challenging task. We show how the bonding contribution equation, a quantitative relation between surface structure and adsorption energy, can be utilized for rational catalyst design. Dozens of catalysts were efficiently designed, and full DFT calculations demonstrate that they possess excellent activities.

The increasing consumption of fossil fuel due to industrialization and motorization results in the energy problem being one of the most important challenges in the 21st century[1]. In the last few decades, many approaches were proposed to solve this problem, such as solar cell[2], photocatalysis[3], electrolyser[4, 5], and fuel cell[6]. However, most of these systems are limited by the low activities or high costs of catalytic materials. Therefore, speeding up the development of novel catalytic materials is generally considered to be the key to solve the energy problem. Considering the rapid development of computing capabilities, one promising approach for fast catalyst developments is to design catalyst candidates based on density functional theory (DFT) calculations; then these catalysts can be synthesized experimentally for further catalytic performance tests. Thus, an effective and rational in silico design method to obtain catalyst structures with desired properties is highly necessary.

Despite the great importance of computational catalyst design, only few design methods were proposed. Nørskov and co-workers suggested a descriptor-based screening method[7, 8] for catalyst searching using DFT calculations. In their work, the optimal value of the descriptor was obtained from the volcano diagram. Using the adsorption energy as a descriptor, they screened the database with large numbers of materials, and some breakthroughs were made; several outstanding catalysts were successfully found for hydrogen evolution[9] and oxygen reduction reaction[10]. Furthermore, in our previous work, we introduced the concept of chemical potential into heterogeneous catalysis[11], based on which the optimal adsorption energy window[12, 13] for good catalysts was located. Using this adsorption energy window, we found a novel active counter electrode material, α-Fe_2O_3, for triiodide reaction in dye-sensitized solar cell[2]. However, further developments are desirable; the screening method may be limited by the size and diversity of screening database.

As suggested in our previous work[14], rational catalyst design is extremely challenging mainly due to the fact that the relation between surface structure and adsorption energy is still not clear. Recently, Sautet and co-workers[15] reported the excellent example of rational catalyst design based on the generalized coordination number[16, 17]. In their work, they introduced a coordination-activity plots to determine the geometric structure of optimal active sites of platinum for oxygen reduction reaction. Herein, we propose a catalyst design approach applicable to a more complicated system namely alloy surfaces based on the bonding contribution equation[18], which is a relation between surface structures and the corresponding adsorption energies introduced in our previous work. Using this equation, several outstanding catalysts of CO oxidation are rationally designed using a simple yet powerful scheme, which are several orders of magnitude more active than traditional platinum catalysts based on the DFT calculations and micro-kinetic modellings.

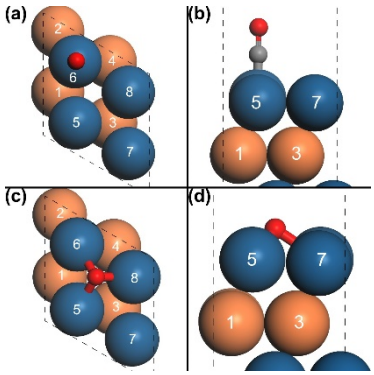

Figure 1. Top views of (a) CO and (c) O, and side views of (b) CO and (d) O, adsorbed on the *p*(2×2) Pt(111) surface. Surface Pt atoms are in blue and with indexes from 5 to 8, while subsurface Pt atoms are highlighted in orange and numbered from 1 to 4. Oxygen and carbon atoms are in red and grey, respectively.

In this work, we chose CO oxidation on Pt-based alloy catalysts for the following reasons: Firstly, CO oxidation is a typical and important reaction in heterogeneous catalysis, and Pt is one of the most active catalysts widely investigated before[19, 20]. Secondly, there are enormous possibilities of alloy structures with different adsorption properties, which is ideal for catalyst design to tune the adsorption energies. Thirdly, some alloy surfaces[21, 22] were reported to possess excellent

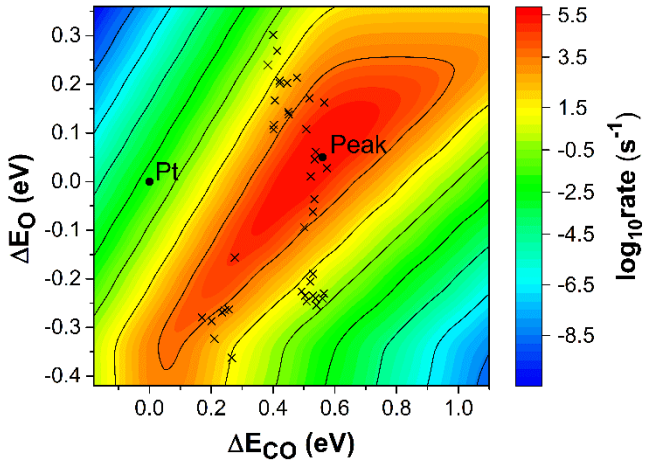

Figure 2. The volcano surface of CO oxidation on close-packed plane surfaces between the adsorption energies of CO (ΔE_{CO}) and O (ΔE_O), and the logarithm of overall reaction rate ($\log_{10} rate$). All the adsorption energies are with respect to the adsorption energies of corresponding adsorbate on Pt(111). The positions of Pt(111), (0,0), and the peak are marked with points labelled Pt and Peak, respectively. The adsorption energies of designed surfaces are marked using crosses, and the points exceed the ranges are not shown (see Table S1 for all the adsorption energies). The activities were calculated under high-temperature conditions (T=600K, PO2=0.33 bar and PCO=0.67 bar).

activities for CO oxidation, suggesting that alloying metal surface is a promising approach to enhance the catalytic activity. In this work, as shown in Figure 1, a *p*(2×2) Pt(111) surface[19, 20] was chosen as the host surface, and only the subsurface (1-4) and surface (5-8) metal atoms were considered to be substituted. Like our previous work, four metals were chosen as alloying solutes, namely Re, Os, Ir, and Pd. In the micro-kinetic modelling, we considered three elementary steps including CO adsorption, O_2 dissociative adsorption[23] and CO oxidation (more details can be found in SI).

One may ask whether the traditional screening methods work in this system. To answer this question, we calculated the number of possibilities of the alloy surfaces: for a Pt(111)-*p*(2×2) surface with four solute metals, in total there are 390625 (5^8) possibilities if only the surface and subsurface atoms are allowed to be substituted. Taking the descriptor-based screening method as an example, a thorough screening of all the possible surfaces needs more than a million DFT calculations, even if the transition states is evaluated using the Brønsted-Evans-Polanyi (BEP) relation[24-28]. This large amount of calculations are very expensive; for complicated systems with more adsorbates, more types solute metals or substitution sites, the catalyst design using the screening method is nearly impossible. Thus, a more rational approach is highly desirable. As stated in our previous work[14], the design problem can be treated as searching for the surface structures with desirable adsorption energies. Therefore, a relation to link the hundreds of thousands of alloy surface structures to the corresponding adsorption energies is the key. In our previous work, an explicit equation was proposed to quantitatively account the surface structures and the adsorption energies, namely the bonding contribution equation[18]. Successful predictions of oxygen adsorption energies on complex alloy surfaces containing up to 4 components were demonstrated, and the generality of this equation was also tested for CO adsorption. The adsorption energy (E_{ad}) of O or CO can be predicted using the equation below:

$$E_{ad} = \sum_{i=1}^{n} g \times c_i \times a_i \qquad (1)$$

where g, c_i and a_i are the generalized parameter, bond-counting contribution factor (BCCF) and the intrinsic bonding ability of solute metal i, respectively. More details in the defination and chemical meaning of these parameters can be found in the original work[18].

We calculated the volcano diagram of CO oxidation (Figure 2) based on the BEP relation and micro-kinetic modelling, similar to the one reported by Nørskov and co-workers[29]. As shown in Figure 2, the peak of the volcano diagram is located at the point with the adsorption energies of 0.56 eV for CO and 0.05 eV for O, respectively, with respect to the adsorption energies on Pt(111). In order to find the most active alloy catalyst, we need to design the alloy structures with adsorption energies near the peak point. Using the bonding contribution equation, the surface structures around the peak point can be obtained arithmetically. We chose the structures with predicted adsorption energies around the peak of volcano diagram with ±0.1 eV. 54 alloy surfaces were obtained according to the adsorption energy intervals mentioned above, and then the adsorption energies of CO and O on these alloy surfaces were calculated using DFT, shown in Figure 2 and Table S1. In Figure 2, the adsorption energies of 31 surfaces are within the adsorption windows, while the others are slightly away. These surfaces close to the peak point in Figure 2 should possess much better activities than Pt(111) based on the volcano diagram.

On these 31 surfaces, full DFT calculations for the reaction were carried out, including explicitly locating the transition states of CO oxidation and O_2 dissociative adsorption, and the activities were obtained using micro-kinetic modelling. The

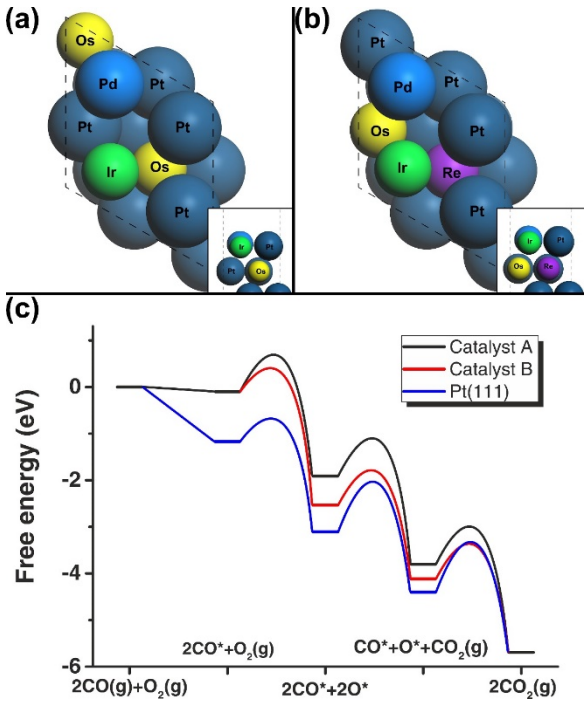

Figure 3. Top views and side views (inset) of (a) catalyst A and (b) catalyst B, and (c) the energy profiles of CO oxidation on catalyst A (black), catalyst B (red) and Pt(111) (blue). The free energies in (c) were obtained using DFT calculations.

Table 1. Surface index, structure, adsorption energies of CO ($\Delta E_{ad}CO$) and O ($\Delta E_{ad}O$), energies of transition states of CO oxidation ($\Delta E_{TS}CO\text{-}O$) and O_2 dissociative adsorption ($\Delta E_{TS}O\text{-}O$), and overall reaction rate of 10 surfaces with highest activities of refined surfaces. The structure is represented by listing the atom symbols of atoms from 1 to 8 as shown in Figure 1. All the energies are with respect to the corresponding energies on Pt(111), and are in eV. The unit of overall rate is s^{-1}.

	Structure	$\Delta E_{ad}CO$	$\Delta E_{ad}O$	$\Delta E_{TS}CO\text{-}O$	$\Delta E_{TS}O\text{-}O$	Rate
A	PtOsOsPtIrPdPtPt	0.54	0.06	0.33	0.31	2.26×10^5
B	OsPtRePtIrPdPtPt	0.54	-0.25	-0.04	0.00	1.79×10^5
C	IrPtRePtIrPdPtPt	0.53	-0.23	-0.02	0.00	1.71×10^5
D	PtIrRePtIrPdPtPt	0.53	-0.19	0.06	0.05	1.01×10^5
E	RePtOsPtIrPdPtPt	0.56	-0.24	0.02	0.06	8.86×10^4
F	OsPtOsPtIrPdPtPt	0.54	-0.24	-0.01	0.00	6.62×10^4
G	OsOsPtPtIrPdPtPt	0.53	-0.06	0.28	0.22	5.60×10^4
H	RePtIrPtIrPdPtPt	0.56	-0.23	0.06	0.06	2.73×10^4
I	PtReIrPtIrPdPtPt	0.57	0.16	0.40	0.48	2.08×10^4
J	PtOsIrPtIrPdPtPt	0.53	-0.04	0.38	0.32	1.66×10^4

energies of transition states and the overall reaction rates of the 10 most active surfaces are listed in Table 1, while the complete results are shown in Table S2. From these results, several striking features can be found: Firstly, the activities of all these surfaces were found in the range from 3.67×10^{2} s^{-1} to 2.26×10^{5} s^{-1}, which are significantly higher than the activity of Pt(111) (Table S2). Therefore, most designed surfaces were found to possess excellent activities, which reduces dramatically the requirement of computation resources compared to screening methods. Furthermore, our design strategy is much more rational than the traditional screenings: giving desiring adsorption properties, the alloy structures are generated using bonding contribution equation without DFT calculations. Secondly, the activities of four surfaces (A, B, C, and D) were found to be at 10^{5} s^{-1} (Table 1), which is the theoretical maximum activity from the volcano diagram. These four surfaces can be classified into two categories based on the adsorption energies of CO and O: For catalyst A, the calculated adsorption energies are very close to the adsorption energies of the peak point, which is the expected outstanding catalyst according to the volcano diagram. Regarding the second category (catalysts B, C and D), the adsorption energies are not in the optimal region, which should have low activities concerning their positions on the volcano diagram. However, the calculated activities with rigorous transition state energies are unexpected to be high, which is beyond the traditional theoretical framework of the volcano diagram from the BEP relation.

To understand the difference between these two groups, we analyzed the activation energies, overall reaction rate, and coverage of CO and O of catalyst A and B, and the results are listed in Table 2. For catalyst A, all the values from the BEP relation are quite close to those from DFT calculations. Thus, catalyst A is a successful example of catalyst design using the volcano diagram based on the BEP relation, and the outstanding activity of catalyst A is derived from the balanced adsorption energies of CO and O. On the other hand, the excellent activity of catalyst B is surprising: According to the volcano diagram, catalyst B should possess an activity of 0.83 s^{-1}, because the adsorption energy of oxygen atom is too strong, resulting in very high coverage of oxygen atom blocking the reaction sites (Table 2). Interestingly, the activity from the DFT calculations is 5 orders of magnitude higher than the one from the BEP relation. To understand the result, we compared the free energy barriers from the BEP relation and DFT calculations as listed in Table 2. Surprisingly, the free energy barriers do not obey the BEP relations: compared to the predicted energy, some differences are evident; the free energy barriers of oxygen dissociative adsorption is 0.31 eV higher from the DFT calculation comparing to that from BEP relation, while for the free energy barrier of CO oxidation, the barrier from the DFT calculation is 0.16 eV lower than that from the BEP relation. According to the free energy profiles of catalyst A and B (Figure 3(c)), the adsorption energy of oxygen on catalyst B is more stable than that of catalyst A, and the barrier of CO oxidation is consequently lower than that on catalyst A. Moreover, the higher oxygen dissociation barrier than the one from the BEP relation results in a slightly low coverage of oxygen, preventing poisoning by oxygen atoms. Due to the presence of adsorption energy window in our strategy, some catalysts that are beyond the BEP relation can also readily be included, which is a great advantage in comparison with other catalyst design approaches. Of course, the energy window in this work can be adjusted and optimized in the future work. In this work, the catalysts were designed with activities very close to that of volcano diagram peak. However, the structures of these catalysts are very complex and hard to synthesize using current methods. Nevertheless, our work is a demonstration of catalyst design using bonding contribution equation; we may apply some constraints to make the surfaces easy to prepare such as restrictions in component numbers and substitution sites. Furthermore, some properties related to surface thermal stabilities can also be considered to pre-screen catalyst candidates in the future.

In this work, using CO oxidation on Pt-based alloys as a model reaction we have demonstrated a catalyst design scheme that is rational. Using the bonding contribution equation, 54 candidate catalysts were designed and the activities of these catalysts were evaluated using micro-kinetic modelling from the full DFT energetics. The activities of these catalysts are much higher than Pt(111). Our scheme allows us to locate not only the catalysts with adsorption energies near the peak of volcano diagram, but also the catalysts that are slightly off from the peak but do not follow the BEP relation, which may pave the way towards rational design of catalysts in general.

Table 2. Comparisons of free energy barriers of CO oxidation (CO-O) and O_2 dissociative adsorption (O-O), reaction rate, and coverages of CO (θ_{CO}) and O (θ_O) from BEP relations and DFT calculation for catalyst A and B. All the energies are with respect to the corresponding energies on Pt(111), and are in eV. The unit of overall rate is s^{-1}.

	Catalyst A		Catalyst B	
	BEP	DFT	BEP	DFT
CO-O	0.82	0.79	0.90	0.74
O-O	0.76	0.78	0.16	0.47
rate	2.20×10^{5}	2.26×10^{5}	0.83	1.80×10^{5}
θ_{CO}	0.45	0.53	2.55×10^{-6}	0.02
θ_O	0.29	0.16	1.00	0.96

Notes and references

1. N. S. Lewis and D. G. Nocera, *Proc. Natl. Acad. Sci.*, 2006, **103**, 15729-15735.
2. Y. Hou, D. Wang, X. H. Yang, W. Q. Fang, B. Zhang, H. F. Wang, G. Z. Lu, P. Hu, H. J. Zhao and H. G. Yang, *Nat. Commun.*, 2013, **4**, 1583.
3. M. R. Hoffmann, S. T. Martin, W. Choi and D. W. Bahnemann, *Chem. Rev.*, 1995, **95**, 69-96.
4. K. Xie, Y. Zhang, G. Meng and J. T. S. Irvine, *J. Mater. Chem.*, 2011, **21**, 195-198.
5. X. Sun, X. Cao and P. Hu, *Science China Chemistry*, 2015, **58**, 553-564.
6. R. Kavanagh, X. M. Cao, W. F. Lin, C. Hardacre and P. Hu, *Angew. Chem. Int. Ed.*, 2012, **51**, 1572-1575.

7. C. H. Christensen and J. K. Norskov, *J. Chem. Phys.*, 2008, **128**, 182503.
8. J. K. Norskov, T. Bligaard, J. Rossmeisl and C. H. Christensen, *Nature Chem.*, 2009, **1**, 37-46.
9. J. Greeley, T. F. Jaramillo, J. Bonde, I. B. Chorkendorff and J. K. Norskov, *Nature Mater.*, 2006, **5**, 909-913.
10. J. Greeley and J. K. Norskov, *J. Phys. Chem. C*, 2009, **113**, 4932-4939.
11. J. Cheng and P. Hu, *Angew. Chem. Int. Ed.*, 2011, **50**, 7650-7654.
12. T. Bligaard, J. K. Norskov, S. Dahl, J. Matthiesen, C. H. Christensen and J. Sehested, *J. Catal.*, 2004, **224**, 206-217.
13. J. K. Norskov, T. Bligaard, A. Logadottir, S. Bahn, L. B. Hansen, M. Bollinger, H. Bengaard, B. Hammer, Z. Sljivancanin, M. Mavrikakis, Y. Xu, S. Dahl and C. J. H. Jacobsen, *J. Catal.*, 2002, **209**, 275-278.
14. Z. Wang and P. Hu, *Phil. Trans. R. Soc. A*, 2016, **374**, 20150078.
15. F. Calle-Vallejo, J. Tymoczko, V. Colic, Q. H. Vu, M. D. Pohl, K. Morgenstern, D. Loffreda, P. Sautet, W. Schuhmann and A. S. Bandarenka, *Science*, 2015, **350**, 185-189.
16. F. Calle-Vallejo, J. I. Martínez, J. M. García-Lastra, P. Sautet and D. Loffreda, *Angew. Chem. Int. Ed.*, 2014, **53**, 8316-8319.
17. F. Calle-Vallejo, D. Loffreda, T. M. KoperMarc and P. Sautet, *Nature Chem.*, 2015, **7**, 403-410.
18. Z. Wang and P. Hu, *Phys. Chem. Chem. Phys.*, 2017, **19**, 5063-5069.
19. A. Alavi, P. Hu, T. Deutsch, P. L. Silvestrelli and J. Hutter, *Phys. Rev. Lett.*, 1998, **80**, 3650-3653.
20. J. Wintterlin, S. Völkening, T. V. W. Janssens, T. Zambelli and G. Ertl, *Science*, 1997, **278**, 1931-1934.
21. J. Xu, T. White, P. Li, C. He, J. Yu, W. Yuan and Y.-F. Han, *J. Am. Chem. Soc.*, 2010, **132**, 10398-10406.
22. X. Liu, A. Wang, X. Wang, C.-Y. Mou and T. Zhang, *Chem. Commun.*, 2008, DOI: 10.1039/B804362K, 3187-3189.
23. H. Wang, Y. Guo, G. Lu and P. Hu, *J. Chem. Phys.*, 2009, **130**, 224701.
24. R. A. v. Santen, M. Neurock and S. G. Shetty, *Chem. Rev.*, 2009, **110**, 2005-2048.
25. V. Pallassana and M. Neurock, *J. Catal.*, 2000, **191**, 301-317.
26. Z. P. Liu and P. Hu, *J. Chem. Phys.*, 2001, **114**, 8244-8247.
27. A. Logadottir, T. H. Rod, J. K. Norskov, B. Hammer, S. Dahl and C. J. H. Jacobsen, *J. Catal.*, 2001, **197**, 229-231.
28. Z. Wang, B. Yang, Y. Wang, Y. Zhao, X. M. Cao and P. Hu, *Phys. Chem. Chem. Phys.*, 2013, **15**, 9498-9502.
29. H. Falsig, B. Hvolbaek, I. S. Kristensen, T. Jiang, T. Bligaard, C. H. Christensen and J. K. Norskov, *Angew. Chem. Int. Ed.*, 2008, **47**, 4835-4839.